Disc-electrospun cellulose acetate butyrate nanofibers show enhanced cellular growth performances

Chen Huang,[1,2,3] Haitao Niu,[2] Chunchen Wu,[3] Qinfei Ke,[1] Xiumei Mo,[3] Tong Lin[2]

[1]College of Textiles, Donghua University, Shanghai 201620, China
[2]Australian Future Fibres Research and Innovation Centre, Institute for Frontier Materials, Deakin University, Geelong, Victoria 3216, Australia
[3]Biomaterials and Tissue Engineering Laboratory, College of Chemistry, Chemical Engineering and Biotechnology, Donghua University, Shanghai 201620, China

Abstract: Cellulose acetate butyrate nanofibers were prepared separately by two electrospinning techniques; a needleless electrospinning using a disc as spinneret and a rotary drum as collector and a conventional needle electrospinning using a rotary drum as collector. Compared to the needle-electrospun nanofibers, the disc-electrospun nanofibers were coarser with a wider diameter distribution. Both fibers had a similar surface morphology and they showed no difference in chemical components, but the disc-electrospun nanofibers were slightly higher in crystallinity. The productivity of disc electrospinning was 150 times larger than that of needle electrospinning. The disc-electrospun nanofiber mats were found to have a three dimensional fibrous structure with an average pore size of 9.1 μm, while the needle-electrospun nanofibers looked more like a two-dimensional sheet with a much smaller average pore size (3.2 μm). Fibroblasts and Schwann cells were cultured on the fibrous matrices to assess the biocompatibility. The disc-electrospun nanofiber webs showed enhanced cellular growth for both fibroblasts and Schwann cells, especially in a long culture period. © 2012 Wiley Periodicals, Inc. J Biomed Mater Res Part A: 101A: 115–122, 2013.

Key Words: needleless electrospinning, nanofibers, three-dimensional tissue scaffold, fibroblasts, Schwann cells

How to cite this article: Huang C, Niu H, Wu C, Ke Q, Mo X, Lin T. 2013. Disc-electrospun cellulose acetate butyrate nanofibers show enhanced cellular growth performances. J Biomed Mater Res Part A 2013:101A:115–122.

INTRODUCTION

Electrospun nanofibers are typically prepared to have a nonwoven-like fibrous structure. They are highly porous with excellent pore interconnectivity and large specific surface area. Electrospun nanofibers are easy to be functionalized through adding functional chemicals, polymers or nanomaterials to polymer solution for electrospinning. These unique properties along with the extra functions brought by the polymer materials have made electrospun nanofibers imperative for applications in areas as diverse as tissue engineering, filtration, energy conversion and storage, reinforcement, sensor, and many others.[1–6]

Electrospun nanofibers produced by needle electrospinning technique (i.e., electrospinning using a needle like spinneret) have been widely studied as tissue scaffolds for the repair/regeneration of ligaments, skins, vascular grafts, nerve guide conduits, and bones.[7–12] They show better support of cell growth than other types of synthetic tissue scaffolds including those having a similar fibrous structure but made of conventional fibers. Structurally, electrospun nanofiber mats are comparable to native scaffolds, that is extracellular matrices (ECMs),[13] which is the main reason leading to the excellent scaffolding performance. However, needle-electrospun nanofiber mats have a tightly packed fibrous structure with pores typically in the range from tens of nanometers to several microns. Cells on such a dense porous structure are much easier to grow along the surface rather than infiltrate into the fibrous matrix. As a result, the nanofiber membranes are primarily suitable as a two-dimensional (2D) tissue scaffold for applications such as in endothelialization.

For many tissue engineering applications, three-dimensional (3D) tissue scaffolds are essential, especially for engineering bone, vascular and dermal tissues.[14] 3D tissue scaffolds vary from 2D scaffolds in that they function as a preformed ECM to support cells to migrate and attach inside the scaffold so that a new 3D tissue can be formed eventually. The pores in 3D tissue scaffolds play a vital role in mediating cell infiltration and growth, and facilitating the exchange of nutrition media and metabolites. The optimal

pore size for 3D tissue scaffolds varies depending on the types of cells and tissues. For example, the pores of 300–400 μm in size are most favorable for culturing bone cells, while the optimal pore range for fibroblasts is 6–20 μm.[15–17]

Considerable efforts have been made recently to develop 3D nanofibrous tissue scaffolds, with a preference to introduce large pores directly through an electrospinning process. Large pores have been created by the incorporation of a spacer agent, such as sacrificial nanofibers through a coelectrospinning technique[18] or salt particles,[19] into nanofiber mats, and after a postelectrospinning treatment to remove the spacers, fibrous mats with a 3D tissue scaffold feature were acquired. Large pores were also formed by introducing coarse fibers into nanofiber webs.[20] A special collector also has been designed to directly collect fibers into a 3D fibrous structure.[21] However, these fibrous matrices either lack uniformity or can only be produced in small quantities due to the use of needle electrospinning.

Recently, needleless electrospinning has appeared as a new electrospinning mode to produce nanofibers on large scales.[22–24] Needleless electrospinning is different to needle electrospinning in that nanofibers are electrospun directly from an open fluid surface without using a needle-like spinneret, and multiple jets are formed from a compacted liquid surface without the confinement of capillary effect that is typically associated with needle electrospinning. The production rate of needleless electrospinning can be tens or even hundreds of times that of conventional needle electrospinning (0.3 g/h), because each needle nozzle can typically produce one polymer jet at one time for needle electrospinning.[23] However, the systematic study of cell growth on needleless electrospun nanofibers has less been found in the research literature.

In the recent study, we found that when a needleless electrospinning was used to produce cellulose acetate butyrate (CAB) nanofibers, the fibrous matrix obtained showed a 3D tissue scaffold feature with an enhanced cell growth performance. Nanofibers produced also showed a much larger production rate when compared with needle electrospinning. In this article, we for the first time report on needleless electrospinning of 3D fibrous tissue scaffolds and their cell culture performance. Fibroblasts and Schwann cells were used for biocompatibility test. For comparison, nanofiber webs were also prepared using a needle electrospinning setup.

MATERIALS AND METHODS
Materials
Cellulose acetate butyrate (CAB, viscosity average molecular weights $M_n \approx 70,000$), was obtained from Aldrich. Acetone (Chem-Supply) and N, N'-dimethylformamide (DMF, Chem-Supply) are of reagent grade. All chemicals were used as received. Rat fibroblasts were donated by Barwon Health Hospital, Australia. Rat Schwann cells (SCs, CRL-2768) and culture media were obtained from American Type Culture Collection (ATCC). All other reagents used for cell culture were purchased from Gibco Life Technologies, USA.
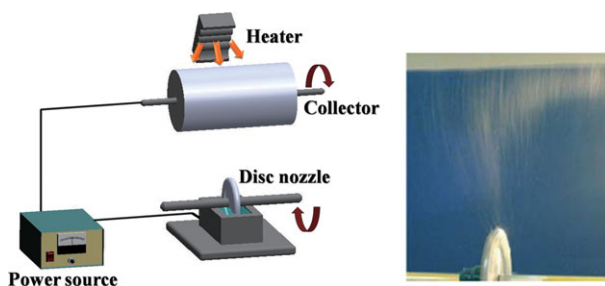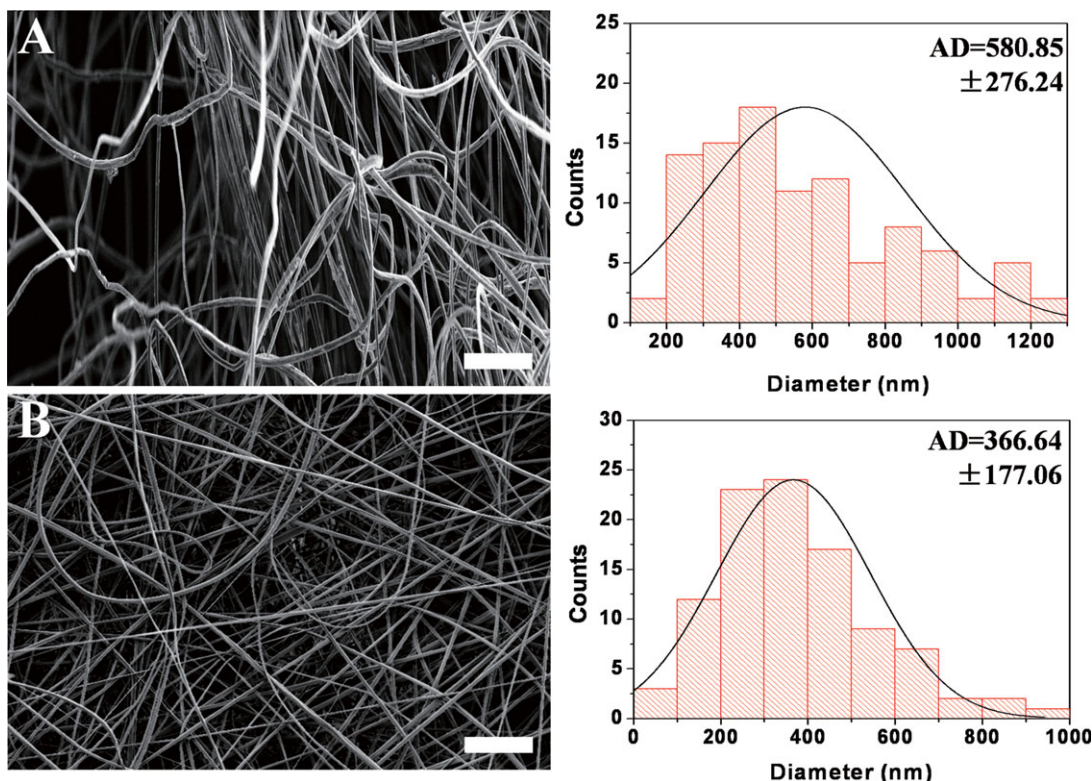

FIGURE 1. Apparatus for disc electrospinning and a photo of the electrospinning process. [Color figure can be viewed in the online issue, which is available at wileyonlinelibrary.com.]

Electrospinning
Disc electrospinning and needle electrospinning were performed using purpose made electrospinning setups.[23,25] CAB (12 wt %) in acetone/DMF (2/1, vol/vol) was used. Figure 1 illustrates the needleless electrospinning setup, which contains a rotary aluminum disc spinneret, a Teflon solution vessel, a high voltage direct-current power supply (ES50P-20W/DAM, Gamma High Voltage Research, USA) and a grounded drum collector. The disc nozzle was 2 mm in thickness and 8 cm in diameter with a beveled edge, and the radius of the beveled curve was about 0.5 mm. During electrospinning, the vessel was filled with CAB solution so that nearly half of the spinneret was immersed in the polymer solution, and the unimmersed part of the spinneret was covered with a thin layer of the CAB solution via rotation. With the rotation of the spinneret, the polymer solution was loaded onto the spinneret surface constantly, which led to the continuous generation of polymer jets/filaments. To facilitate the removal of solvent residues from the freshly collected nanofibers, two electrical heaters (surface temperature 120°C) were set beside the drum collector with a distance of 10 cm. During electrospinning, unless specified the applied voltage, the electrospinning distance and the rotating speed of the disc nozzle were controlled at 50 kV, 16 cm and 40 rpm, respectively. For the needle electrospinning, the applied voltage, the electrospinning distance and the flow rate were set at 15 kV, 16 cm, and 1.2 mL/h, respectively. After electrospinning, CAB fibers were kept in vacuum at 80°C overnight to remove the trace solvent residue.

Characterizations
Fiber and cell morphologies were observed under a field emission scanning electron microscope (SEM, Zeiss SUPRA 55VP). The fiber diameter was measured based on the SEM images using image analysis software *ImageJ* (National Institutes of Health, USA). Electrospun nanofiber mats ($n = 3$) were cut into 3 × 3 cm^2 for measurement of pore size and distribution using a CFP-1100-AI capillary flow porometer (Porous Materials Int.). Galwick with a surface tension of 20.1 dynes/cm (PMI) was used as the wetting agent for the measurement. Fourier transform infrared spectroscopy (FTIR) spectra were recorded on a VERTEX 70 FTIR spectrometer (Bruker Biosciences Pty) and wide angle X-ray diffraction were obtained on an X-ray diffractometer (Riga Ku, Japan) using CuKα

FIGURE 2. SEM images and the histogram of fiber diameter distribution for, (A) disc-electrospun nanofibers, (B) needle-electrospun nanofibers. (Scale bar = 5 μm). [Color figure can be viewed in the online issue, which is available at wileyonlinelibrary.com.]

radiation ($\lambda = 1.5418$ Å) at 40 kV and 40 mA. The water contact angle of nanofiber mats were measured using a water contact angle meter (KSV CAM200 Instruments).

Cell culture, cell viability, and cell morphology

Fibroblasts were cultured in Roswell Park Memorial Institute-1640 (RPMI-1640) and Schwann cells were cultured in Dulbecco's modified Eagle's medium (DMEM) under a standard culture condition (i.e., 37°C, in a humidified atmosphere containing 5% CO_2 and 95% air). Both media were supplemented by 10% fetal bovine serum (FBS) and 1% antibiotic–antimycotic. After sterilization in an autoclave at 121°C for 15 min, the CAB nanofiber samples were washed with sterilized phosphate buffered saline (PBS, 10 mM, pH 7.4) for three times, and once with culture medium. The scaffold samples were then punched into a circular shape (14 mm in diameter) and placed individually into a 24-well culture plate. A stainless ring was used to secure the scaffold sample in the wells. Cells were then seeded onto the scaffolds at a density of 2.0×10^4 cells/well and the culture medium was replenished every 3 days.

Cell attachment and viability were assessed with cell counting kit-8 (CCK-8, Sigma-Aldrich). Briefly, the scaffolds were rinsed with PBS. After moving to another 24-well TCP, the scaffolds were immersed with 400 mL of fresh culture medium in each well. CCK-8 reagent (40 μL) was added into each well, and incubation was then performed for 2 h according to the reagent instruction. This allowed the WST-8 (2-(2-methoxy-4-nitrophenyl)-3-(4-nitrophenyl)-5-(2,4-disulfo-phenyl)-2H-tetrazolium, monosodium salt) in CCK-8 being reduced by cellular dehydrogenases to form an orange formazan product that is soluble in tissue culture medium. Coloration is thus developed and the absorption value is positively proportional to the number of living cells. An aliquot (150 mL) of incubated medium was pipetted into a 96-well TCP for optical absorption measurement at 450 nm using an Enzyme-labeled Instrument (MK3, Thermo, USA). The same volume of culture medium and CCK-8 reagent without cells was also incubated as the background. The CCK-8 test 4 h after cell seeding was used to evaluate the cell attachment, and the tests on days 1, 3, 5, and 7 after incubation were employed for measuring the cell viability. Tissue culture polystyrene (TCP) wells were also used as control and all experiments were performed repeatedly for six times.

To observe cells under SEM, the cultured matrices were rinsed with sterilized PBS for three times to remove medium and unviable cells, and then fixed by immersing the cell carrying matrices in 2.1% (wt/vol) glutaraldehyde/ PBS for 4 h at room temperature. After rinsing with PBS for three times, the matrices were immersed in a 2% (wt/vol) aqueous OsO_4 solution for 20 min. The matrices were then immersed in a 1% (wt/vol) aqueous tannic acid solution for 10 min and rinsed with 20% ethanol/water solution. The matrices were finally freeze-dried (Labconco Freezone 2.0).

Statistical analysis

Statistical analysis was performed using Origin (Origin lab, USA). Values ($n = 6$) were averaged and expressed as
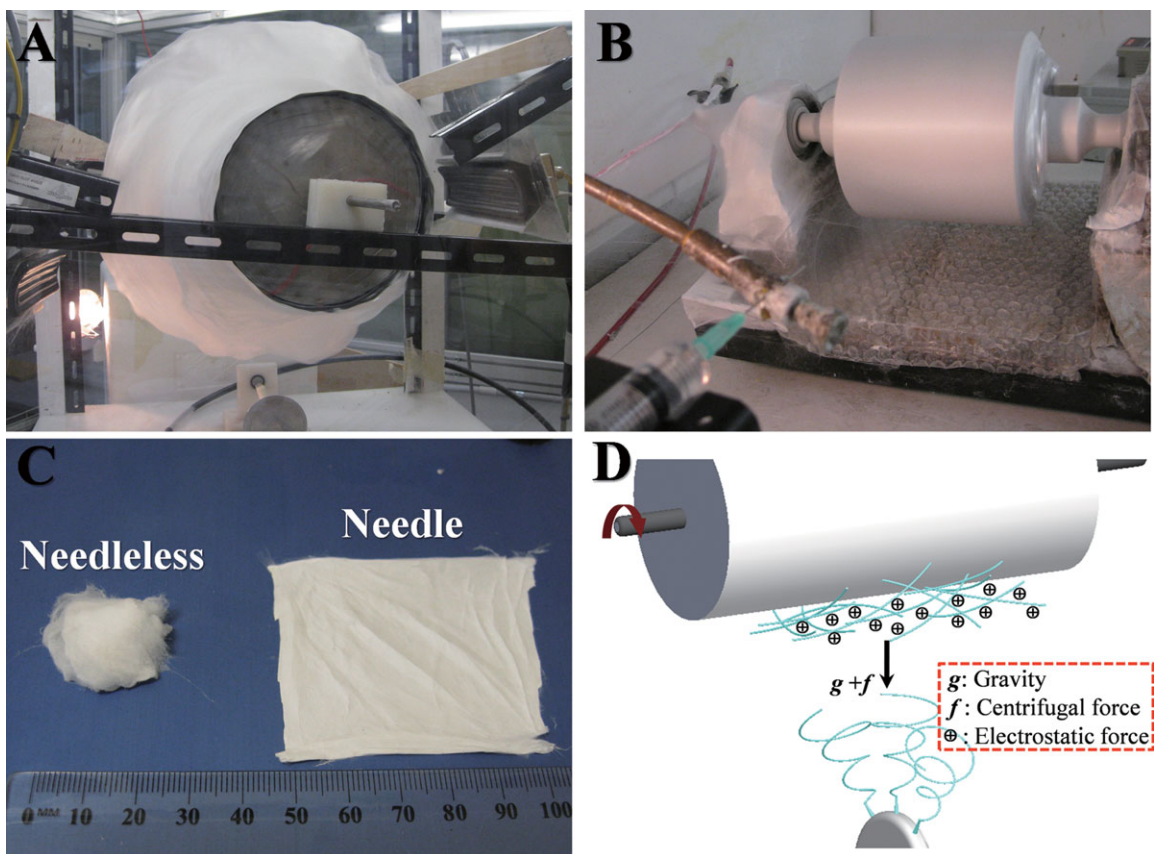
FIGURE 3. Photos of CAB nanofibers produced by, (A) disc electrospinning setup (15 min), and (B) needle electrospinning setup (3 h). (C) Appearance of nanofiber mat produced from the two setups, (D) Proposed formation mechanism of 3D fibrous structure. [Color figure can be viewed in the online issue, which is available at wileyonlinelibrary.com.]

means ± standard deviation (SD). Statistical differences were determined by the analysis of one way ANOVA and differences were considered statistically significant at $p < 0.05$.

RESULTS AND DISCUSSION
### Morphology of CAB nanofiber webs
Figure 2 shows the SEM images of CAB fibers electrospun from disc and needle electrospinning techniques. The disc-electrospun nanofibers looked uniform in fiber morphology and contained no beads, which were similar to those electrospun from the needle electrospinning. At the concentration of 12%, CAB was electrospun into smooth fibers without a parallel-grooved surface feature.[26] The needle-electrospun nanofibers had an average diameter of 367 nm. Coarser fibers (average diameter 581 nm) with a wider diameter distribution were produced from disc electrospin-

ning. This is in good accordance with the report by Niu et al.[23] who used disc electrospinning to electrospin polyvinyl alcohol nanofibers. The coarser nanofibers with wider diameter distribution compared to needle electrospinning were attributed to the widely distributed electrical field intensity on the disc edge.

Figure 3 shows the appearance of nanofiber mats electrospun from the two different electrospinning techniques. The needleless electrospun nanofibers had a loose fibrous structure on the collector [Fig. 3(A)]. However, fibers produced by the needle electrospinning adhered firmly on the drum collector, forming a sheet like fibrous membrane [Fig. 3(B)], and such a fibrous characteristic was not changed by adjusting the rotating speed of the drum. Upon taking the nanofiber webs off the collectors, the original fibrous characteristics were remained without deformation. As shown in Figure 3(C), the nanofiber web produced by

TABLE I. Pore Diameter and Productivity of CAB Nanofiber Mats

CAB Nanofiber Mats	Mean Pore Diameter ± SD (µm)	Largest Pore Diameter (µm)	Smallest Pore Diameter (µm)	Productivity (g/h)
Disc-spun	9.100 ± 4.513	44.248	0.402	22.40
Needle-spun	3.193 ± 1.001	6.478	0.434	0.14
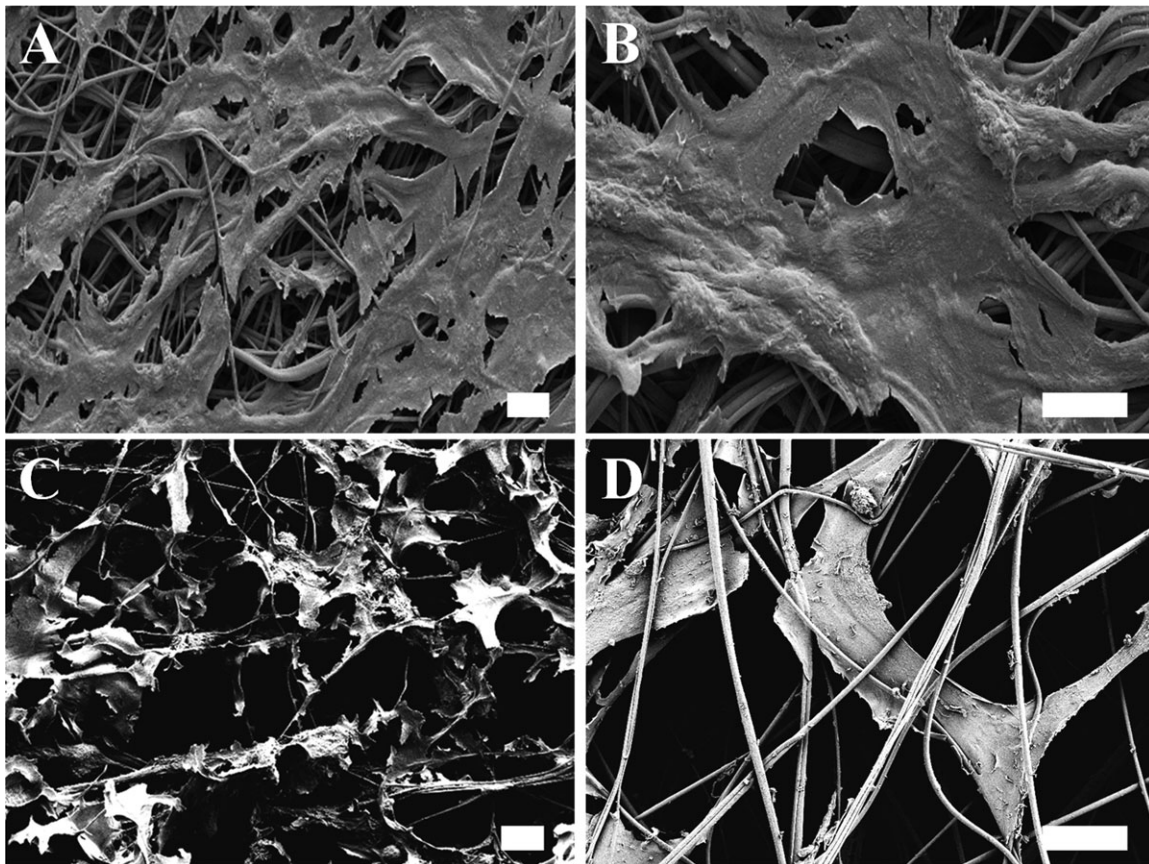
FIGURE 4. SEM images of fibroblasts growing on, (A, B) needle-electrospun nanofiber mats, (C, D) disc-electrospun nanofiber mats. (Scale bar = 10 μm).

the disc electrospinning has a candy floss-like structure, a typical characteristic of 3D fibrous scaffolds.[21] For the nanofiber web prepared from the needle electrospinning, a highly packed nanofiber sheet was formed.

The pore size of nanofiber mats is listed in Table I. For the disc-electrospun fiber mats, the average pore diameter measured was 9.1 μm, which was much larger than that of the needle-electrospun nanofiber mats (pore diameter 3.2 μm). The SEM images in Figure 2 also reveal that disc-electrospun nanofibers have a much lower fiber density when compared with the needle-electrospun nanofibers. As expected, the disc electrospinning had a nanofiber production rate of 22.40 g/h, which was much higher than that of the needle electrospinning (0.14 g/h), although a single disc was employed for needleless electrospinning.

Cell viability

Two types of cells, fibroblast and Schwann cells, were used to assess the biocompatibility of the CAB nanofiber mats. Fibroblasts were selected as they can be easily regulated by the contact guidance from culture substrates.[27] Our previous study has found that Schwann cells exhibiting prompt proliferation on electrospun CAB nanofibers and the growth behavior could be readily regulated though the control of fiber orientation.[26]

Figure 4 shows the SEM images of fibroblasts on CAB nanofiber scaffolds after 7 days of culture. All cells spread well on the scaffolds, regardless of the pore size and fiber density. On the needle-electrospun nanofiber mats [Fig. 4(A,B)], cells grew mainly on the scaffold surface and no cell infiltration was observed into the fiber matrix. However, fibroblasts on the disc-electrospun scaffolds showed quite different growth behavior [Fig. 4(C)]. Instead of growing on the top surface or falling into the bottom of the scaffold, cells were found to integrate in the fiber matrix. Clear cellular infiltration can be observed under high magnification in Figure 4(D). Some of the cells were found to migrate into the porous matrix, showing a similar structure to cells on the native ECMs.[28]

Schwann cells were also found to grow well on the nanofiber scaffolds. As shown in Figure 5, most of the Schwann cells have a cell cytoskeleton-elongated bipolar shape, which is known to be conducive for peripheral nerve repair. Similar to the fibroblasts, the Schwann cells grew only on the surface of the needle-electrospun nanofiber mats [Fig. 5(A,B)], but they migrated into the disc spun nanofiber matrix [as marked by the arrows in Fig. 5(D)]. Unlike the fibroblasts, which looked to float on the matrix surface, most Schwann cells penetrated, at least partially into the fiber matrix. This is probably because Schwann cells have a narrow bipolar structure, which is easier to
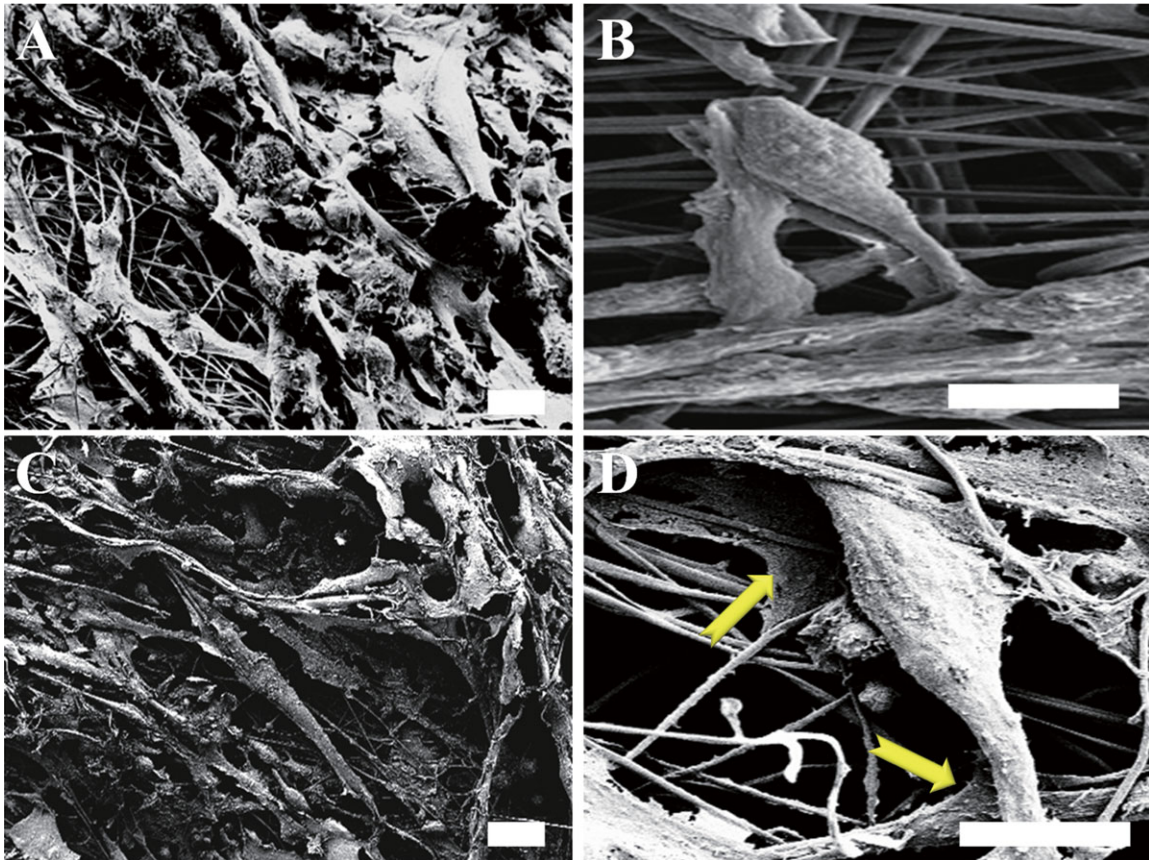
FIGURE 5. SEM images of Schwann cells growing on, (A, B) needle-electrospun nanofiber mats, and (C, D) disc-electrospun nanofiber mats. (Cell infiltration was marked by the arrows, scale bar = 10 μm). [Color figure can be viewed in the online issue, which is available at wileyonlinelibrary.com.]

migrate into the pores [Fig. 5(C)]. In comparison, fibroblasts are flat and they are more sensitive to the ambient environment. These results also indicate that fibrous structure has a significant effect on cell growth performance.
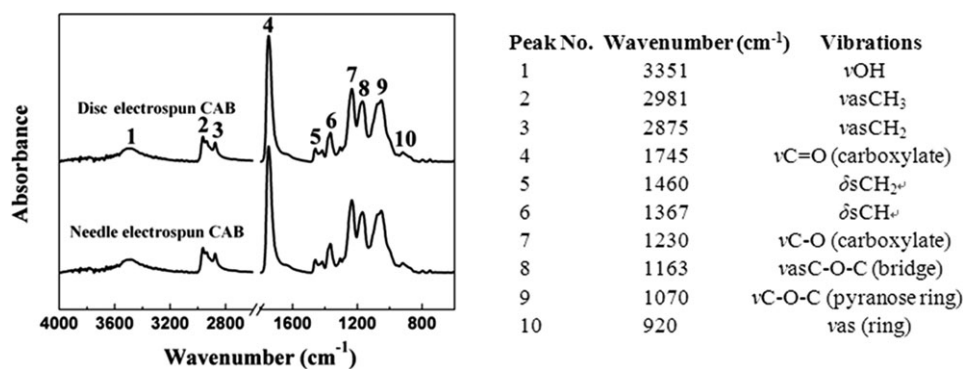
Cells on scaffolds are normally expected to experience three discernible stages: initial adhesion, spreading, and proliferation. The cell attachment to the electrospun nanofiber mats was assessed quantitatively using CCK-8 assay.

The number of attaching cells is proportional to the optical absorption of the colored enzyme extracted from the sample. Figure 6 summarizes the initial attachment and viability of cells in different incubation periods.

Both cells at an early stage (4 h) showed better attachment to the tissue culture polystyrene (TCP), when compared with the nanofiber mats. This was presumably due to the hydrophobic nature of CAB. The water contact angle of
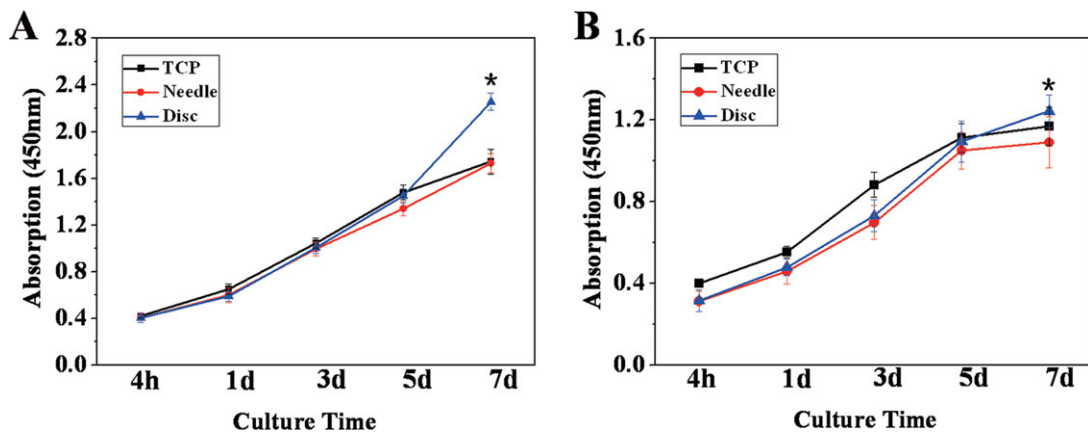
FIGURE 6. Cell attachment and proliferation of (A) fibroblasts and (B) Schwann cells on TCP, needle-electrospun nanofiber mats, and disc-electrospun nanofiber mats. [Color figure can be viewed in the online issue, which is available at wileyonlinelibrary.com.]

Peak No.	Wavenumber (cm⁻¹)	Vibrations
1	3351	νOH
2	2981	νasCH$_3$
3	2875	νasCH$_2$
4	1745	νC=O (carboxylate)
5	1460	δsCH$_2$
6	1367	δsCH
7	1230	νC-O (carboxylate)
8	1163	νasC-O-C (bridge)
9	1070	νC-O-C (pyranose ring)
10	920	νas (ring)

FIGURE 7. FTIR spectra and characteristic vibrations of CAB nanofibers electrospun from two different methods. The characteristic vibrations were assigned according to literatures.[30–33]

electrospun CAB nanofiber mats was 120°. Such hydrophobic surfaces have been reported to retard the cell adhesion.[29]

Cell number increased with increasing the culture date, indicating the proliferation of cells on the scaffolds. With 5 days, cell number on the TCP was similar to that on the nanofiber mats, and there was no difference between disc- and needle-electrospun mats regarding the cell growth performance.

The most significant change (p = 0.05) was found on day 7. For fibroblasts, the cell number on the TCP and the needle spun nanofiber webs maintained a positive linear growth throughout 7 days. However, the cell growth on the disc spun nanofiber mats tended to increase in growth rate, and this became more apparent on day 7 [Fig. 6(A)]. This led to much larger number of cells growing on the disc-electrospun nanofiber webs compared with that on needle-spun nanofibers. At day 7, the CCK-8 absorption values for the disc- and the needle-electrospun nanofibers were 2.258 and 1.729, respectively, indicating that the former had 30.60% more fibroblasts than the later.

For Schwann cells, cell growth on the TCP and needle-spun nanofibers was slowed down considerably from day 5 to day 7. However, on the disc-electrospun nanofiber mats, cell number still increased, albeit at a slightly lower rate. From day 5 to 7, cells on the disc-electrospun nanofiber mats increased by 13.59%, which was much higher than that on the needle-electrospun nanofiber samples (3.79%).

The overall growth trend for the cells on needle-electrospun nanofiber mats was similar to TCP, but the disc-electrospun nanofiber mats were much different, especially on day 7. The difference in cell growth trend should derive from different cell-matrix interaction. If cells can only grow on the surface of a tissue scaffold, which is the case of the needle-electrospun nanofiber web or TCP, their growth would enable the cells to cover the entire surface gradually. When cells can migrate into the matrix, they can grow and proliferate with larger surface area and pore space. The fact that fibroblasts growing on the disc-electrospun nanofiber mat shows larger growth rate suggests that the cell proliferate at a larger rate when they infiltrate into the nanofibrous matrix. The disc-electrospun nanofibrous webs offer a 3D porous environment to support cell infiltration and proliferation. The slightly reduced growth rate for the Schwann cells on day 7 suggests that the pores in the disc spun nanofiber matrix could be still small for Schwann cells.

Formation mechanism of the 3D structure

The mechanism of forming 3D fibrous structure during disc electrospinning was proposed as illustrated in Figure 3(D). During electrospinning, numerous charged nanofibers were deposited on the collector. The rapid deposition of fibers led to charge accumulation on the collector, forming a loosely packed fibrous structure. Because the fibers were still wet, they tended to stick together in the connected sections. Heated by the two heaters around the fibers collected were rapidly solidified which resulted in bonded fiber structure. The bonded fibers can effectively prevents the fibrous structure from collapsing, leading to a highly loose, but structurally stable 3D fibrous matrix. In contrast, the low fiber production rate of needle electrospinning allowed the fibers electrospun to have sufficient time to dissipate electrical charges on the collector. This led to a layer-by-layer deposition of fibers into a dense sheet structure.

FTIR and XRD results

FTIR and XRD were also performed to examine the influence of electrospinning methods on nanofiber composition and crystalline structure. Figure 7 shows the FTIR spectra
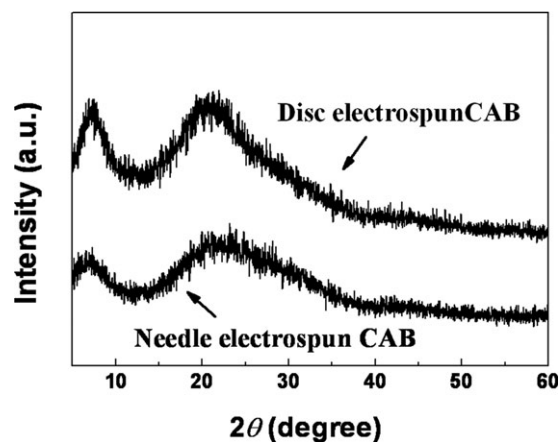
FIGURE 8. XRD patterns of CAB nanofibers produced from the two electrospinning methods.

of electrospun CAB nanofibers. There was no difference in FTIR found between the two nanofiber mats. It has been reported that needle electrospinning has no influence on the chemical composition of nanofibers electrospun. The same FTIR feature between the needle- and disc-electrospun nanofibers indicated that disc electrospinning method should have no influence on the chemical composition of polymer.

Figure 8 shows the X-ray diffraction pattern of the CAB nanofibers. There was no obvious difference in the main diffraction peaks of the nanofibers. The broad diffraction peak at around 21.2° suggested that CAB nanofibers were largely in an amorphous state. However, the disc-electrospun nanofibers showed a stronger peak at 7.2°. The crystallinity calculated based on the XRD result indicated that the disc-electrospun nanofibers had a slightly higher crystallinity (41.08%) than the needle-electrospun ones (32.55%).

CONCLUSIONS

A highly porous 3D nanofibrous scaffold has been produced directly by a needleless electrospinning technique using a disc as the spinneret and a rotary drum as the collector. In comparison with conventional needle electrospinning, the disc electrospinning showed 150 times higher nanofiber production rate. The disc-electrospun nanofiber webs showed enhancement in the cellular growth of both fibroblast and Schwann cells, especially in a long culture period (7 days). The disc electrospinning showed no influence on the chemical composition of polymer electrospun, but slightly increased the crystallinity. These results suggests that needleless electrospinning is advantageous in producing 3D nanofibrous tissue engineering scaffolds with large productivity, which could form a promising technique platform for production of 3D tissue scaffolds for engineering various tissues including bones, cartilages, muscles, and many others.

REFERENCES

1. Li D, Xia Y. Electrospinning of nanofibers: Reinventing the wheel? Adv Mater 2004;16:1151–1170.
2. Cao H, Liu T, Chew SY. The application of nanofibrous scaffolds in neural tissue engineering. Adv Drug Deliv Rev 2009;61:1055–1064.
3. Ramakrishna S, Fujihara K, Teo W-E, Yong T, Ma Z, Ramaseshan R. Electrospun nanofibers: Solving global issues. Mater Today 2006;9:40–50.
4. Wang X, Drew C, Lee SH, Senecal KJ, Kumar J, Samuelson LA. Electrospun nanofibrous membranes for highly sensitive optical sensors. Nano Lett 2002;2:1273–1275.
5. Bergshoef MM, Vancso GJ. Transparent nanocomposites with ultrathin, electrospun nylon-4,6 fiber reinforcement. Adv Mater 1999;11:1362–1365.
6. Fang J, Niu H, Lin T, Wang X. Applications of electrospun nanofibers. Chinese Sci Bull 2008;53:2265–2286.
7. Yin Z, Chen X, Chen JL, Shen WL, Hieu Nguyen TM, Gao L, Ouyang HW. The regulation of tendon stem cell differentiation by the alignment of nanofibers. Biomaterials 2010;31:2163–2175.
8. Blackwood KA, McKean R, Canton I, Freeman CO, Franklin KL, Cole D, Brook I, Farthing P, Rimmer S, Haycock JW, et al. Development of biodegradable electrospun scaffolds for dermal replacement. Biomaterials 2008;29:3091–3104.
9. Stitzel J, Liu J, Lee SJ, Komura M, Berry J, Soker S, Lim G, Van Dyke M, Czerw R, Yoo JJ, et al. Controlled fabrication of a biological vascular substitute. Biomaterials 2006;27:1088–1094.
10. Chew SY, Mi R, Hoke A, Leong KW. Aligned protein–polymer composite fibers enhance nerve regeneration: A potential tissue-engineering platform. Adv Funct Mater 2007;17:1288–1296.
11. Matthews JA, Wnek GE, Simpson DG, Bowlin GL. Electrospinning of collagen nanofibers. Biomacromolecules 2002;3:232–238.
12. Gupta D, Venugopal J, Mitra S, Giri Dev VR, Ramakrishna S. Nanostructured biocomposite substrates by electrospinning and electrospraying for the mineralization of osteoblasts. Biomaterials 2009;30:2085–2094.
13. Langer R, Vacanti JP. Tissue engineering. Science 1993;260:920–926.
14. Moroni L, de Wijn JR, van Blitterswijk CA. 3D fiber-deposited scaffolds for tissue engineering: Influence of pores geometry and architecture on dynamic mechanical properties. Biomaterials 2006;27:974–985.
15. Tsuruga E, Takita H, Itoh H, Wakisaka Y, Kuboki Y. Pore size of porous hydroxyapatite as the cell-substratum controls BMP-induced osteogenesis. J Biochem 1997;121:317–324.
16. Karageorgiou V, Kaplan D. Porosity of 3D biomaterial scaffolds and osteogenesis. Biomaterials 2005;26:5474–5491.
17. Lowery JL, Datta N, Rutledge GC. Effect of fiber diameter, pore size and seeding method on growth of human dermal fibroblasts in electrospun poly(ε-caprolactone) fibrous mats. Biomaterials 2010;31:491–504.
18. Baker BM, Gee AO, Metter RB, Nathan AS, Marklein RA, Burdick JA, Mauck RL. The potential to improve cell infiltration in composite fiber-aligned electrospun scaffolds by the selective removal of sacrificial fibers. Biomaterials 2008;29:2348–2358.
19. Kim TG, Chung HJ, Park TG. Macroporous and nanofibrous hyaluronic acid/collagen hybrid scaffold fabricated by concurrent electrospinning and deposition/leaching of salt particles. Acta Biomaterialia 2008;4:1611–1619.
20. Park SH, Kim TG, Kim HC, Yang D-Y, Park TG. Development of dual scale scaffolds via direct polymer melt deposition and electrospinning for applications in tissue regeneration. Acta Biomaterialia 2008;4:1198–1207.
21. Blakeney BA, Tambralli A, Anderson JM, Andukuri A, Lim DJ, Dean DR, Jun HW. Cell infiltration and growth in a low density, uncompressed three-dimensional electrospun nanofibrous scaffold. Biomaterials 2011;32:1583–1590.
22. Yarin AL, Zussman E. Upward needleless electrospinning of multiple nanofibers. Polymer 2004;45:2977–2980.
23. Niu H, Lin T, Wang X. Needleless electrospinning. I. A comparison of cylinder and disk nozzles. J Appl Polym Sci 2009;114:3524–3530.
24. Lu B, Wang Y, Liu Y, Duan H, Zhou J, Zhang Z, Wang Y, Li X, Wang W, Lan W, et al. Superhigh-throughput needleless electrospinning using a rotary cone as spinneret. Small 2010;6:1612–1616.
25. Lin T, Wang H, Wang X. The charge effect of cationic surfactants on the elimination of fibre beads in the electrospinning of polystyrene. Nanotechnology 2004;15:1375–1381.
26. Huang C, Tang Y, Liu X, Sutti A, Ke Q, Mo X, Wang X, Morsi Y, Lin T. Electrospinning of nanofibres with parallel line surface texture for improvement of nerve cell growth. Soft Matter 2011;7:10812–10817.
27. Walboomers XF, Croes HJE, Ginsel LA, Jansen JA. Contact guidance of rat fibroblasts on various implant materials. J Biomed Mater Res 1999;47:204–212.
28. Kim B-S, Mooney DJ. Development of biocompatible synthetic extracellular matrices for tissue engineering. Trends Biotechnol 1998;16:224–230.
29. Arima Y, Iwata H. Effect of wettability and surface functional groups on protein adsorption and cell adhesion using well-defined mixed self-assembled monolayers. Biomaterials 2007;28:3074–3082.
30. Kondo T, Sawatari C. A Fourier transform infra-red spectroscopic analysis of the character of hydrogen bonds in amorphous cellulose. Polymer 1996;37:393–399.
31. Ilharco LM, Brito de Barros R. Aggregation of pseudoisocyanine iodide in cellulose acetate films: Structural characterization by FTIR. Langmuir 2000;16:9331–9337.
32. Park JW, Tanaka T, Doi Y, Iwata T. Uniaxial drawing of poly[(R)-3-hydroxybutyrate]/cellulose acetate butyrate blends and their orientation behavior. Macromol Biosci 2005;5:840–852.
33. Ilharco LM, Garcia AR, Lopes da Silva J, Vieira Ferreira LF. Infrared approach to the study of adsorption on cellulose: Influence of cellulose crystallinity on the adsorption of benzophenone. Langmuir 1997;13:4126–4132.